

Estimation of methane flux offshore SW Taiwan and the influence of tectonics on gas hydrate accumulation

P.-C. CHUANG¹, T. F. YANG¹, W.-L. HONG¹, S. LIN², C.-H. SUN³, A. T.-S. LIN⁴, J.-C. CHEN², Y. WANG⁵ AND S.-H. CHUNG⁵

¹*Department of Geosciences, National Taiwan University, Taipei, Taiwan;* ²*Institute of Oceanography, National Taiwan University, Taipei, Taiwan;* ³*Exploration & Development Research Institute, CPC, Miaoli City, Miaoli County, Taiwan;* ⁴*Institute of Geophysics, National Central University, Jhongli, Taiwan;* ⁵*Central Geological Survey, MOEA, Taipei, Taiwan*

ABSTRACT

Widely distributed bottom simulating reflectors (BSRs) imply the potential existence of gas hydrates offshore southwestern Taiwan. To compare the distribution of methane concentrations along passive and active margins in the region, bottom waters and cored sediments were collected during four cruises from 2005 to 2006. The results reveal that sites with high methane concentrations are predominantly distributed in the active margin and site GS5 is the only site that contains very high methane concentrations in the passive margin of studied area. Anomalously high methane fluxes still can be obtained from the calculation of diffusive methane flux, although there might be some gas leakage during or after sampling procedures. The profiles of methane and sulfate concentration reveal very shallow depths of the sulfate–methane interface (SMI) at some sites. There is evidence that sulfate reduction is mainly driven by the process of anaerobic methane oxidation. Thus, sulfate fluxes can be used as a proxy for methane fluxes through the use of diffusion equations; and the results show that the fluxes are very high in offshore southwestern Taiwan. The depths of the SMI are different at sites GH6 and C; however, both methane profiles reveal parallel methane gradients below the SMI. This might be because of methane migration to surface sediments from the same reservoir with the same diffusion rates. Although BSRs are widely distributed both in the active margin and in the passive margin, most sites with high methane concentrations have been found in the active margin. Therefore, the specific tectonic settings in offshore SW Taiwan might strongly control the stability of gas hydrates, and thus affect the methane concentrations and fluxes of the sediments and sea waters. Furthermore, the carbon isotopic composition of methane shows that a biogenic gas source is dominant at shallower depth; however, some thermogenic gases might be introduced through the fracture/fault zones from deeper source in the active region of studied area.

Key words: anaerobic methane oxidation, gas hydrate, methane flux, sulfate reduction, Taiwan

Received 24 August 2010; accepted 29 August 2010

Corresponding author: Tsanyao F. Yang, Department of Geosciences, National Taiwan University, No. 1, Sec. 4, Roosevelt Road, Taipei 106, Taiwan.

E-mail: tyang@ntu.edu.tw. Tel: +886 2 3366 5874. Fax: +886 2 2363 6095.

Geofluids (2010) 10, 497–510

INTRODUCTION

Gas hydrates are naturally occurring solids, nonstoichiometric clathrates, stable at relatively low temperature and high pressure conditions. They can be found in the permafrost of polar region and in sedimentary strata of continental deep sea areas and are typically composed of natural gas, mainly methane, within a rigid lattice of water molecules. Accordingly, gas hydrates have been considered as potential energy resources for the future and an important

component of the global carbon cycle (Kvenvolden 1998; Sloan 1998; Dickens 2001; Milkov 2004).

Offshore southwestern Taiwan is located in the collision zone between the Luzon arc of Philippine Sea Plate and Eurasian continental plate (Teng 1990). In this area, an active accretionary prism has been formed by collision and a deformation front separates the distinctive fold-and-thrust structures of the convergent zone and horst-and-graben structures of the passive margin. Under this tectonic setting, the temperature and pressure conditions

allow the formation of gas hydrates in marine sediments from water depths of 500 to 3000 m (Liu *et al.* 2006). In previous geophysical studies, many bottom simulating reflectors (BSRs) were recognized in offshore southwestern Taiwan. These BSRs may indicate that gas hydrates are widely distributed at depths of 700–3000 mbsf (meters beneath the seafloor) (Chi *et al.* 1998; Schnürle *et al.* 1999, 2002; Chow *et al.* 2000; Liu *et al.* 2006). Some morphological features, such as mud volcanoes, might be closely linked to gas hydrates and the regional tectonic settings. For instance, at least 50 submarine mud volcanoes and diapirs have been identified by Chiu *et al.* (2006) and onshore mud volcanoes found in southwestern Taiwan along faults or other tectonic structures might be closely related to gas hydrate dissociation (Yang *et al.* 2003, 2004; You *et al.* 2004; Yeh *et al.* 2005; Chao *et al.* 2010; Sun *et al.* 2010).

The area investigated in the present work is characterized by intense fluid circulation (Liu *et al.* 2006). Gassy sediments and mud volcanoes, detected by chirp sonar and seismic reflection profiles, occur from the accretionary wedge to the passive continental margin of China. From seismic profiles, identified gas chimney structures may form conduits to allow the upward flow of fluids. When fluids move through highly permeable faults, such higher temperature fluids can also affect surrounding sediments and then result in destabilization of gas hydrate (Chiu *et al.* 2006). Pecher (2002) proposed that liquids and gases derived from dissociated gas hydrates would affect the compositions of sea water and sediments near to the venting areas. Hence, methane anomalies in seawater may occur in correspondence with hydrates in offshore SW Taiwan.

Previous studies have suggested that methane concentrations play an important role in gas hydrate investigations. Very high methane concentrations (up to $133\,354\ \mu\text{l l}^{-1}$ at site G23 of cruise ORI-697) and very shallow depth of the sulfate–methane interface (hereafter abbreviated to SMI) (<100 cm at site G23 of cruise ORI-697 and N8 of cruise ORI-718), indicate high methane fluxes below the seafloor, were found in offshore SW Taiwan (Chuang *et al.* 2006; Yang *et al.* 2006; Yang 2008). Moreover, high dissolved sulfide concentration, very fast sulfate reduction rate (Lin *et al.* 2006) and very depleted carbon isotope values of authigenic carbonates (from -54‰ to -43‰) have also been reported (Huang *et al.* 2006). These geochemical data strongly support the geophysical profiles of mud volcanoes, gassy sediments, and BSRs and strongly suggest the occurrence of gas hydrates in this area. These geochemical anomalies are predominantly found in the active margin. Such geochemical signatures in the passive margin of this region, however, have not been reported.

In this study, the methane concentrations of cored samples and bottom water from four cruises are reported (ORI-758, ORI-765, ORI-792, and ORI-804). Particularly, the

studied area is extended to the passive margin through cruises ORI-765, ORI-792, and ORI-804. The new results show the distribution of methane concentrations in the passive margin in comparison with the results of Lin *et al.* (2006) who estimated the methane and sulfate fluxes in active margin, with their results only showing a range of calculated values. To identify the methane and sulfate fluxes of each site both in active margin and in passive margin, methane and sulfate fluxes have been calculated based on methane and sulfate profiles, respectively. Selected samples with high methane concentrations were analyzed for carbon isotopic composition to constrain their gas sources. Finally, the variances of methane concentrations, the depth of SMI, methane fluxes, and the data of $\delta^{13}\text{C}_{\text{CH}_4}$ are compared in different tectonic settings within the studied area to assess whether the tectonic environments influence the stability of gas hydrates in offshore SW Taiwan.

STUDY AREA AND METHODS

Offshore southwestern Taiwan is located in the transition from a zone of subduction to a zone of collision. This area is in the frontal area of the accretionary wedge of the Luzon Arc and the China passive continental margin subduction–collision system (Liu *et al.* 2006; Lin *et al.* 2008). A deformation front separates the passive China continental margin and the submarine Taiwan accretionary wedge. A series of fold-and-thrust structures are the dominant features in the accretionary wedge province to the east. These may provide good conduits for gases and liquids venting upward to the surface. According to Chiu *et al.* (2006), there are at least 50 submarine mud volcanoes and diapirs that have been identified in chirp sonar and seismic reflection profile data. In addition, the formation of onshore mud volcanoes reported by Yang *et al.* (2004), Chao *et al.* (2010), and Sun *et al.* (2010) might be associated with offshore mud volcanoes. In contrast to the active margin, normal faults are the main structural feature in the passive margin. The geological setting of offshore SW Taiwan has been well documented in previous studies (Huang *et al.* 2006; Liu *et al.* 2006; Lin *et al.* 2008).

In this study, cored sediments have been systematically collected for compositional analysis of dissolved and pore-space gases through four cruises: ORI-758, ORI-765, ORI-792, and ORI-804 during the period of 2005–2006. The ocean bottom water samples were collected from core top water through cruises ORI-765, ORI-792, and ORI-804. The sampling sites are shown in Fig. 1 and Table 1.

Bottom water and sediment samples were collected to analyze the dissolved methane concentration and methane concentration in the pore space. Sediment samples were collected by both gravity core samplers (30–100 cm long) and piston core samplers (300–500 cm long). To simplify the sampling procedures and reduce the required volume

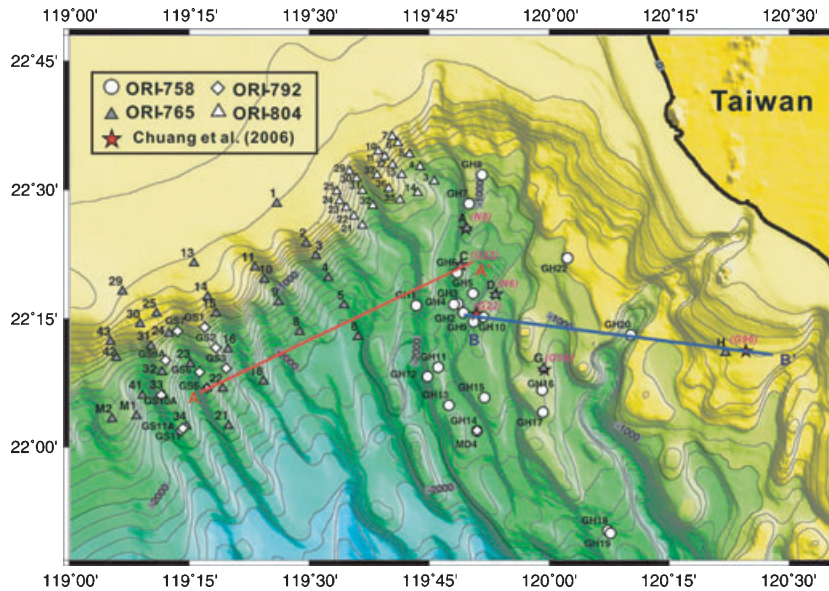


Fig. 1. Bathymetric map of offshore Taiwan. Different symbols with colors represent sites of different cruises.

of sediments, in this study, the sampling methods were improved and modified in comparison with those used previously (Chuang *et al.* 2006).

After core retrieval, a 200 -ml vial filled up with the core top water sample was sealed with a butyl rubber stopper and capped with an aluminum crimp for the measurement of methane. Next, the sediment core was cut into a 1 -m-long section, and then 5 ml sediment sample was taken by a 5 -ml syringe at around 25 -cm intervals of every core section depending on different cruises. The sediment for methane determination was transferred immediately into a 20 -ml glass vial filled up with a saturated sodium chloride solution to prevent further microbiological activity. In addition, the gas solubility will decrease if the salinity of the solution increases (Milkov *et al.* 2004). A saturated sodium chloride solution can also be used to transfer methane into the gas phase. The vials were sealed with butyl rubber stoppers and capped with aluminum crimps.

Before analysis, 5 ml of sodium chloride solution was removed and replaced by the same volume of pure nitrogen gas as the headspace. Afterward, the sample vials were shaken by hand and put in an ultrasonic bath for 30 min at room temperature (25°C) to let hydrocarbon gases partition into the headspace. With a syringe, about 3 ml of gas was removed from the headspace for analysis and the same volume of sodium chloride solution was injected to replace the volume of the gas removed to provide a pressure balance within the sediment vial.

Gas was introduced into a gas chromatograph (GC) (SRI 8610C) equipped with both thermal conductivity (TCD) and flame ionization (FID) detectors. Different components of the gas were separated in GC (injection temperature 30°C, held isothermal for 2 min, ramped to

250°C at 120°C min⁻¹). The system utilized two carrier gases, hydrogen and argon. Hydrogen was supplied by a hydrogen generator for use in the FID and in one TCD; while the other TCD utilized argon supplied by a cylinder tank. In general, most gas components analyzed in this system have analytical errors <5% with low detection and quantification limits (Lee *et al.* 2005, 2008). Results of dissolved methane concentrations are reported relative to the volume of seawater from which the gases were extracted [i.e., nanoliters of gas per liter of seawater (nl l⁻¹)] and methane concentrations of cored sediments are reported relative to wet sediment from which the gases were extracted [i.e., microliters of gas per liter of wet sediment (μl l⁻¹)]. These units followed those used by, for example, Suess *et al.* (1999) and Kvenvolden & Lorenson (2000). These may be unconventional units, but they are convenient for expressing gas concentrations that result from the sampling procedure and for comparison with previously reported results.

Some selected headspace samples of cored sediments were measured for δ¹³C_{CH₄} by GC isotopic ratio mass spectrometer in the Laboratory of Exploration & Development Research Institute, CPC of Taiwan. The precision of repeated analyses (1σ) was ±0.5‰. The details of the carbon isotopic analysis were described by Sun *et al.* (2010).

RESULTS

Methane concentrations in bottom waters

Dissolved methane concentrations in bottom waters are shown in Table 2. Core top water samples from the cruise ORI-804 contain low dissolved methane concentrations

Table 1 Locations, types and lengths of cores, and water depths of the sites in this study.

Sites of ORI-758	Longitude (N)	Latitude (E)	Core type	Water depth (m)	Core length (cm)	Sites of ORI-765	Longitude (N)	Latitude (E)	Core type	Water depth (m)	Core length (cm)
GH1	119°43.34'	22°16.61'	P	1489	170	2	22°23.86'	119°29.57'	G	451	162
GH2	119°49.27'	22°15.759'	P	1422	383	3	22°22.41'	119°30.76'	G	886	182
GH3	119°48.58'	22°16.81'	P	1670	380	4	22°19.82'	119°32.34'	G	1405	14
GH4	119°48.08'	22°16.73'	P	1677	130	5	22°16.62'	119°34.31'	G	1925	222
GH5	119°50.48'	22°18.00'	P	1726	80	6	22°12.95'	119°36.04'	G	2069	142
GH6	119°48.46'	22°20.42'	P	1316	410	8	22°13.51'	119°28.73'	G	1791	142
GH7	119°49.98'	22°28.47'	P	927	236	9	22°17.00'	119°26.08'	G	1506	182
GH8	119°51.61'	22°31.86'	P	1088	415	10	22°19.54'	119°24.33'	G	1114	62
GH9	119°51.73'	22°15.26'	P	1083	80	11	22°21.05'	119°23.13'	G	756	102
GH10	119°50.54'	22°14.68'	P	1216	315	14	22°17.59'	119°17.21'	G	518	52
GH11	119°46.12'	22°09.39'	P	1487	455	15	22°15.66'	119°18.27'	G	889	103
GH12	119°44.76'	22°08.29'	P	1585	79	16	22°11.48'	119°19.76'	G	1276	156
GH13	119°47.42'	22°04.94'	P	1668	423	18	22°07.74'	119°24.18'	G	1799	155
GH14	119°50.97'	22°01.92'	P	1648	423	21	22°02.54'	119°19.84'	G	1635	182
GH15	119°51.89'	22°05.83'	P	1353	440	22	22°06.89'	119°19.09'	G;P	1125	130/427
GH16	119°59.12'	22°06.69'	P	1019	263	24	22°13.30'	119°12.37'	G	800	151
GH17	119°59.25'	22°04.12'	P	997	172	25	22°15.66'	119°10.78'	G	471	102
GH18	120°07.38'	21°50.25'	P	1762	463	30	22°14.41'	119°08.72'	G	523	147
GH19	120°07.70'	21°49.94'	P	1756	430	31	22°11.84'	119°10.08'	G	1120	97
GH20	120°10.24'	22°13.16'	P	1020	447	32	22°08.85'	119°11.48'	G	1257	142
GH22	120°02.29'	22°22.13'	P	639	113	33	22°06.15'	119°11.62'	G	1214	143
						34	22°02.46'	119°14.56'	G	1688	170
						41	22°06.08'	119°09.03'	G	1798	42
						42	22°10.47'	119°05.76'	G	1136	110
						A	22°25.61'	119°49.69'	P	908	285
						C	22°21.18'	119°48.88'	P	1221	445
						D	22°17.80'	119°53.22'	P	1165	414
						H	22°11.07'	120°22.09'	P	407	516
						M1	22°03.69'	119°08.29'	P	1379	458
						M2	22°03.33'	119°05.23'	P	1275	475
Sites of ORI-792	Longitude (N)	Latitude (E)	Core type	Water depth (m)	Core length (cm)	Sites of ORI-804	Longitude (N)	Latitude (E)	Core type	Water depth (m)	Core length (cm)
GS1	22°14.03'	119°16.84'	P	1058	363	3	22°31.11'	119°45.59'	G	1243	26
GS2	22°11.64'	119°18.23'	P	939	386	4	22°32.79'	119°43.82'	G	824	128
GS3	22°09.22'	119°19.55'	P	1444	359	5	22°34.22'	119°42.48'	G	728	136
GS5	22°06.917'	119°17.14'	P	1124	42	10	22°34.56'	119°38.58'	G	319	34
GS6	22°08.81'	119°16.20'	P	1104	450	11	22°33.95'	119°39.39'	G	537	106
GS7	22°13.59'	119°13.43'	P	953	263	13	22°31.86'	119°41.54'	G	986	160
GS9A	22°10.15'	119°11.92'	P	960	430	14	22°29.75'	119°43.53'	G	1084	132
GS10A	22°06.10'	119°11.40'	P	1252	386	21	22°25.92'	119°36.58'	G	1182	157
GS11	22°01.97'	119°13.90'	P	1618	443	22	22°27.01'	119°35.53'	G	992	122
GS11A	22°02.22'	119°14.11'	P	1648	1075	23	22°28.02'	119°34.55'	G	800	149
MD4	22°01.95'	119°50.96'	P	1648	680	24	22°28.77'	119°33.72'	G	577	108
						25	22°29.88'	119°33.35'	G	360	29
						29	22°32.24'	119°34.95'	G	625	84
						30	22°31.40'	119°35.85'	G	914	144
						31	22°29.98'	119°36.61'	G	1129	122
						35	22°28.90'	119°41.31'	G	1018	170
						36	22°30.24'	119°39.88'	G	678	62
						37	22°31.77'	119°38.42'	G	623	38
						GS5	22°06.91'	119°17.14'	P	1126	445

G, gravity core; P, piston core.

Table 2 Dissolved methane concentrations of bottom seawaters and water column in offshore southwestern Taiwan.

ORI-765 cruise bottom seawater	CH ₄ (nl l ⁻¹)	ORI-792 cruise bottom seawater	CH ₄ (nl l ⁻¹)	ORI-804 cruise bottom seawater	CH ₄ (nl l ⁻¹)	ORI-792 cruise water column	CH ₄ (nl l ⁻¹)	Depth (m)
a	3882	GS1	366	3	5.59	GS5-1	251	5
c	516	GS3	235	4	b.d.l.	GS5-2	231	100
8	20	GS5	4 137 250	5	b.d.l.	GS5-3	346	300
18	155	GS6	236	6	b.d.l.	GS5-4	60	600
16	85	GS7	400	7	b.d.l.	GS5-5	40	950
15	27	GS9A	204	11	b.d.l.	GS5-6	95	1020
14	26	GS10A	839	12	b.d.l.	GS5-7	166	1070
25	37	GS11	178	14	b.d.l.	GS5-8	86	1100
24	15	GS11A	203	22	b.d.l.	GS5-9	149	1120
22-c	25	MD4	135	23	b.d.l.			
22-p	314			25	b.d.l.			
21	53			29	b.d.l.			
34	68			30	b.d.l.			
33	55			31	b.d.l.			
31	23			32	b.d.l.			
30	25			36	b.d.l.			
42	49			37	b.d.l.			
M1	22			GS5	b.d.l.			
M2	38							

b.d.l., below detection limit.

and all of them are less than sea water background values, even below detection limits in some cases. Figure 2 shows the distribution of dissolved methane concentrations of bottom waters obtained from different cruises in this study. The results of sites A, C, 22-p of cruise ORI-765, and all sites of cruise ORI-792 are much higher than the value of normal sea water (about 50 nl l⁻¹), particularly site GS5 containing anomalously high methane concentrations (ca. 4 137 250 nl l⁻¹). However, the results of dissolved methane concentrations in the water column at site GS5 do not show an increasing trend with depth or unusually high values at depth. It is thus suspected that there may be some lateral migration of the samplers at different water depths while sampling, or that water column samples are not directly above the site GS5 because of strong current in the area, and so do not show high methane values as expected.

Methane concentrations and isotopic compositions in cored sediments

Methane concentrations in cored sediments of this study are listed in Table 3. Ethane can only be detected from sites N6, N8, G22, and G96 and most C₂₊ gases are below detection limit (1 ppm). Here, only methane concentration data are listed. Methane concentrations of cored sediments at some sites contain higher values at greater depths (over 1000 µl l⁻¹), e.g., GH3, GH6, GH10, GH16 of cruise ORI-758; A, C, D, H of cruise ORI-765; and GS5 of cruise ORI-792. Especially at sites GH6, GH10 of cruise

ORI-758 and A, C, D, H of cruise ORI-765, methane concentrations are >10 000 µl l⁻¹ which are higher than the gas hydrate and gas venting rich area on the Blake Ridge in offshore southwestern United States (Kvenvolden & Lorenson 2000; Lorenson & Collett 2000). Methane concentrations at other sampling sites display no difference with increasing depths (between 10⁰ and 10² µl l⁻¹).

Some of the sites with high methane concentrations are located in the vicinity of sites with extremely high methane concentrations found in offshore SW Taiwan (Chuang *et al.* 2006; Yang *et al.* 2006). For instance, sites A, C, D of cruise ORI-765 are at the same locations as sites N8 of cruise ORI-718, G23 of cruise ORI-697, N6 of cruise ORI-718 and sites GH6, GH3, GH10 of cruise ORI-758 are close to sites G23, G22 of cruise ORI-718. Otherwise site H of cruise ORI-765 is close to site G96 of cruise ORI-732 (Figs 3 and 4; Table 3). These observations from different cruises and the same sampling sites of different years indicate that methane venting areas of offshore SW Taiwan are widespread, and there is a sustained methane venting source underneath each site.

The carbon isotopic compositions of methane of some selected gas samples have been analyzed. Figure 5 and Table 4 show the δ¹³C data of CH₄ gases ranging from -28.3‰ to -74.5‰. Those results indicate that biogenic gas is an important source for the samples. However, the isotopic ratio of site G96 is much higher than other samples with a high C₁/(C₂ + C₃) ratio and falls in the area of the mixed zone between biogenic and thermogenic sources (Fig. 5).

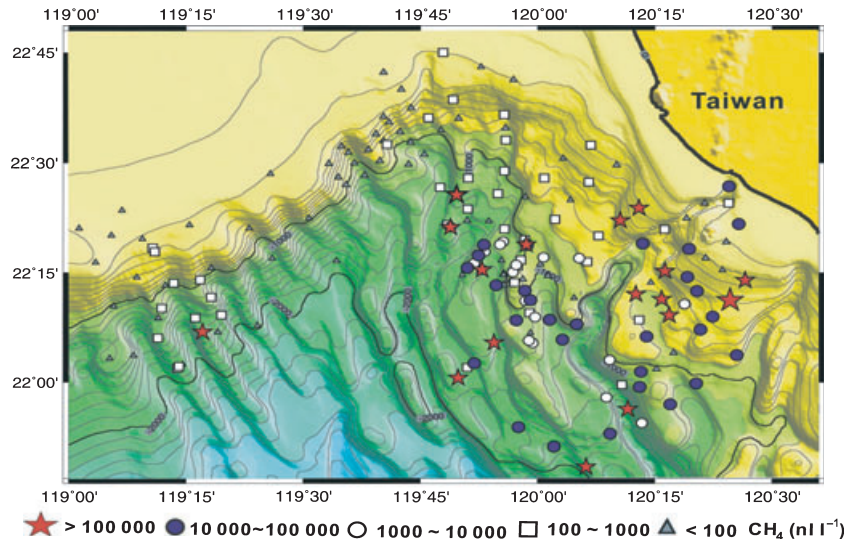
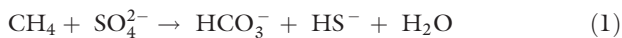


Fig. 2. The distribution of methane concentrations (in nl l^{-1}) in bottom seawaters from offshore southern Taiwan.

DISCUSSION

Methane fluxes in offshore southwestern Taiwan

A SMI can be observed at one depth below which methane tends to increase and sulfate is almost depleted. As methane from the dissociation of gas hydrates migrates upward, anaerobic methane oxidation (AMO) is mediated by a consortium of methanogenic and sulfate-reducing bacteria at the base of sulfate reduction zone (Borowski *et al.* 1996). The net reaction of AMO can be shown as Eqn (1).



The depth of the SMI can be used to imply the amount of methane flux from sediments. If methane flux is high, sulfate reduction rate will be fast and so results in a shallower SMI. Therefore, the depth of the SMI can be a further indicator for the methane flux from buried sediments if there are gas hydrates beneath the sea floor (Borowski *et al.* 1996, 1999).

Methane versus sulfate concentrations profiles of some selected sites are shown in Fig. 3. Dissolved methane concentrations in bottom water and methane concentrations of pore space in deeper sediments are anomalously high at sites G5A, G23 of ORI-697, N6, N8, G22 of ORI-718 cruise and G96 of ORI-732 cruise (Chuang *et al.* 2006), GH3, GH6, GH10 of ORI-758 cruise, A, C, D, H of ORI-765 cruise and GS5 of ORI-792 cruise. The depths of the SMIs in these sites are obviously very shallow (<4 m), so that the methane fluxes at those sites are potentially higher than sites apparently without an SMI.

Lin *et al.* (2006) have reported some calculated methane fluxes and sulfate fluxes of sites distributed in the active margin and concluded that some sites with lower methane

fluxes probably contain high organic carbon contents which result in sulfate depletion. However, the depth of the SMI can only be recognized at six sites (sites: G5A, G22, G23, G96, N6, and N8) (Chuang *et al.* 2006), so that lower methane concentrations of other sites might be the residual methane concentrations after AMO process.

If methane profiles display steep linear gradients just below the SMI, upward diffusive methane fluxes can be calculated from the linear gradients based on Fick's first law (Niewöhner *et al.* 1998). For this reason, methane gradients of sites without the SMI might not be appropriate for fluxes calculations. Therefore, the methane fluxes have been calculated at sites where the SMI can be recognized. It is interesting to note that if it is assumed that the porosity of the sample is 0.6 (Jiang *et al.* 2006), then the highest methane concentration of site G23 of cruise ORI-697 can be converted as 9.08 mm under NTP condition. This value may exceed shipboard saturation levels of methane gas, so probably not only the dissolved gas but also some free gas existed in the pore space. In this case, however, such high values only appear at greater depths in the profiles, and they are below the depth of the concentration gradients which are used for further flux calculation (see Discussion in next session). Therefore, when the concentration values are higher than saturation levels, these are not used to calculate methane fluxes.

Methane flux calculations

Some methane profiles presented in Fig. 3, and Chuang *et al.* (2006) show concave-upward curvatures and methane concentrations become greater with increasing depths. Because of the steep linear gradient below the SMI the upward diffusive fluxes of methane can be inferred (Niewöhner *et al.* 1998). Thus, diffusive methane fluxes from methane gradients have been calculated based on Fick's

Table 3 Maximum and minimum methane concentrations ($\mu\text{l l}^{-1}$) of cored samples at each site in this study.

ORI-758			ORI-765			ORI-792			ORI-804		
cruise	Minimum	Maximum									
GH1	10.3	111	2	0.46	106	GS1	6.30	14.7	3	1.40	2.70
GH2	6.26	60.3	3	2.19	99.5	GS2	1.92	32.5	4	1.30	13.0
GH3	12.8	9552	4	3.17	10.6	GS3	0.78	23.3	5	1.10	1.80
GH4	4.51	13.3	5	1.68	30.3	GS5	1940	7986	10	2.10	3.20
GH5	4.59	18.1	6	2.93	30.4	GS6	19.6	29.8	11	4.10	6.90
GH6	2.36	15 738	8	3.58	8.81	GS7	20.9	213	13	2.00	13.0
GH7	21.4	171	9	0.30	39.3	GS9A	18.2	41.7	14	1.80	11.0
GH8	9.6	31.4	10	66.1	97.8	GS10A	19.7	24.9	21	6.70	21.0
GH9	11.0	26.4	11	11.1	89.1	GS11	1.71	73.6	22	6.70	20.0
GH10	4.47	31 290	14	0.31	2.80	GS11A	1.28	86.1	23	3.10	18.0
GH11	1.72	53.0	15	3.76	12.2				24	6.10	36.0
GH12	4.97	36.5	16	0.55	4.09				25	1.50	4.20
GH13	8.75	421	18	1.93	12.0				29	4.10	7.40
GH14	3.48	67.0	21	3.14	9.56				30	4.00	16.0
GH15	2.38	614	22G	2.18	7.32				31	5.00	21.0
GH16	4.17	2044	22P	16.2	68.5				35	1.00	3.40
GH17	3.62	23.0	24	2.07	4.44				36	0.90	3.20
GH18	6.62	56.1	25	1.63	40.8				37	3.60	7.30
GH19	4.00	55.3	30	2.26	3.41				GS5	5.30	199
GH20	3.45	30.5	31	3.93	11.5						
GH22	5.53	22.7	32	1.68	8.26						
			33	4.12	5.67						
			34	2.58	6.35						
			41	3.14	7.25						
			42	16.2	2.94						
			A	18.7	11 143						
			C	6.06	14 224						
			D	1.37	13 300						
			H	312	20 225						
			M1	1.44	4.11						
			M2	3.98	69.8						

first law assuming steady-state conditions (e.g., Berner 1980):

$$J = -\varphi \cdot D_s \cdot dc/dx \quad (2)$$

In Eqn (2), J is the diffusive flux ($\text{mmol m}^{-2} \text{year}^{-1}$), φ is the porosity (using mean porosity over the depths with steep methane gradients), C is the concentration of methane (mm), x is the depth (m) and D_s is the sediment diffusion coefficient ($\text{m}^{-2} \text{year}^{-1}$). Furthermore, D_s can be calculated from the Eqn (3).

$$D_s = D_0/[1 + n(1 - \varphi)] \quad (3)$$

where D_0 is the tracer diffusion coefficient of methane in seawater ($0.87 \times 10^{-5} \text{ cm}^2 \text{ sec}^{-1}$ at 4°C ; Iversen & Jørgensen 1993) and $n = 3$ for clay-silt sediments (Niewöhner *et al.* 1998). The results of methane flux calculations are listed in Table 5. Note that methane fluxes cannot be calculated from profiles at sites where no SMI has been observed.

There might be some gas leakage during core recovery and sampling procedures, so that the results of flux calculations

would be underestimated. Even though the calculated fluxes cannot truly represent *in situ* methane fluxes, the minimum values still show anomalously high methane fluxes at some sites in offshore SW Taiwan, e.g., sites: G23 of cruise ORI-697, N8 of cruise ORI-718, GH3, GH10 of cruise ORI-758 and A of cruise ORI-765. Furthermore, the anomalously high methane flux at site G23 of cruise ORI-697 ($4.18 \times 10^{-2} \text{ mmol cm}^{-2} \text{ year}^{-1}$) is more than one order of magnitude greater than the estimated fluxes of other gas hydrate and upwelling study areas in the world [e.g., Blake Ridge: $1.8 \times 10^{-3} \text{ mmol cm}^{-2} \text{ year}^{-1}$ (Borowski *et al.* 1996); Hydrate Ridge: $7.9 \times 10^{-4} \text{ mmol cm}^{-2} \text{ year}^{-1}$ (ODP Sites 994); $7.6 \times 10^{-4} \text{ mmol cm}^{-2} \text{ year}^{-1}$ (ODP Sites 995); $7.2 \times 10^{-4} \text{ mmol cm}^{-2} \text{ year}^{-1}$ (ODP Sites 997) (Dickens 2001); $6.15 \times 10^{-3} \text{ mmol cm}^{-2} \text{ year}^{-1}$ (Namibia) (Niewöhner *et al.* 1998)].

Calculation of a proxy for methane fluxes (sulfate fluxes)

Although the delayed sampling procedure after core retrieval might result in lower methane concentrations, *in situ* methane fluxes can be calculated from pore water sulfate concentrations. To perform the calculation, however, it must be proved that sulfate is consumed by methane. This

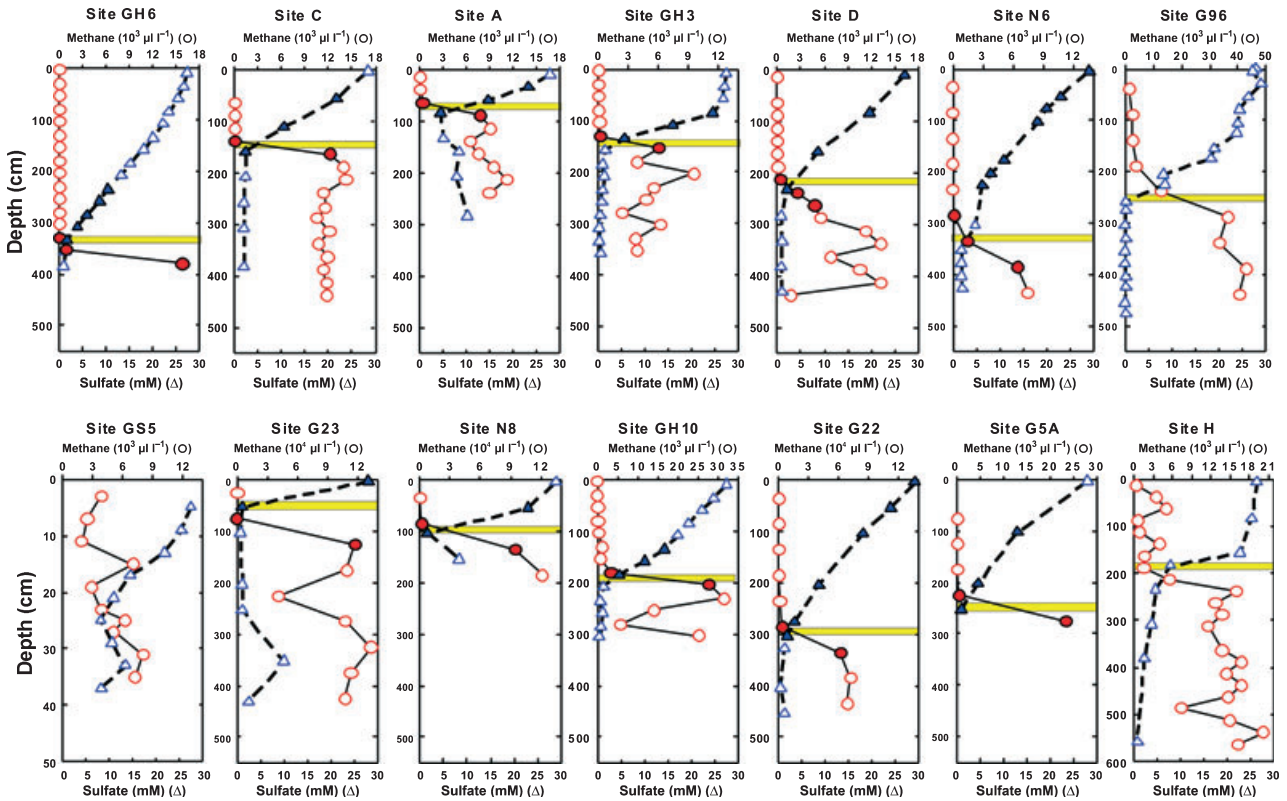
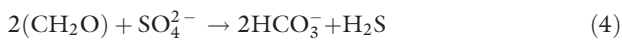


Fig. 3. Some selected profiles of methane concentrations of pore space in cored samples and dissolved sulfate concentrations in pore water. Methane concentrations are represented by circles, and sulfate concentrations are represented by triangles. The points used for the calculation of the methane and sulfate flux are shown as solid symbols. The yellowish area marked in different profiles shows the range of the depths of sulfate–methane interface. The data of sulfate concentrations are from Lin *et al.* (2006).

is because, in addition to the AMO process, sedimentary organic matters also can react with interstitial sulfate to reduce the sulfate within anoxic marine sediments. The net reaction of this process is shown below.



According to the shape of linear sulfate gradients, it is possible to infer that sulfate depletion is mainly controlled by the AMO reaction rather than by the flux of sedimentary organic matter from above. The equation of coupled sulfate–methane reaction (Eqn 1) shows a one-to-one stoichiometry. The linear part of sulfate gradient has been calculated to indicate methane fluxes in many studies (Borowski *et al.* 1996; Niewöhner *et al.* 1998; Hensen *et al.* 2003).

Geochemical profiles for cored samples are plotted in Fig. 3 with corresponding sulfate concentrations (Lin *et al.* 2006) in pore water and methane concentrations in pore space. Because the linear sulfate gradient above the SMI can be observed from each site, it is possible that sulfate is mainly consumed by methane. In addition, the total organic carbon (TOC) content is <1% in the study area (Lin *et al.* 2006). Sivan *et al.* (2007) proposed that pore water sulfate is mainly depleted by AMO reactions if

the TOC content in sediments is <5%. Moreover, a recent study has shown that the carbon isotopic data of methane and dissolved inorganic carbon are both depleted around the depths of the SMI, which can prove the occurrence of AMO in the study area (Chen *et al.* 2008).

Although there might be strong advection in the fluids at the center of the vent sites, steep gradients from sulfate and methane profiles that can imply species which diffuse upward or downward (Borowski *et al.* 1996; Niewöhner *et al.* 1998). Hence, Fick's first law has been applied (Eqns 1 and 2) to calculate the diffusive sulfate fluxes from linear gradients. D_0 of sulfate in seawater at 4°C is $0.56 \times 10^{-5} \text{ cm}^2 \text{ sec}^{-1}$ (Iversen & Jørgensen 1993). Results of estimated sulfate fluxes are shown in Table 5. In comparison with methane fluxes, the discordance of methane flux and sulfate flux appears at each site. The lower methane concentration might result from delayed sampling procedure after core retrieval. Therefore, the calculated methane fluxes all are less than the calculated sulfate fluxes.

The differences of the SMI depths can be used to infer the relative extent of methane fluxes below the sea floor (Borowski *et al.* 1996). Sites with higher sulfate fluxes are

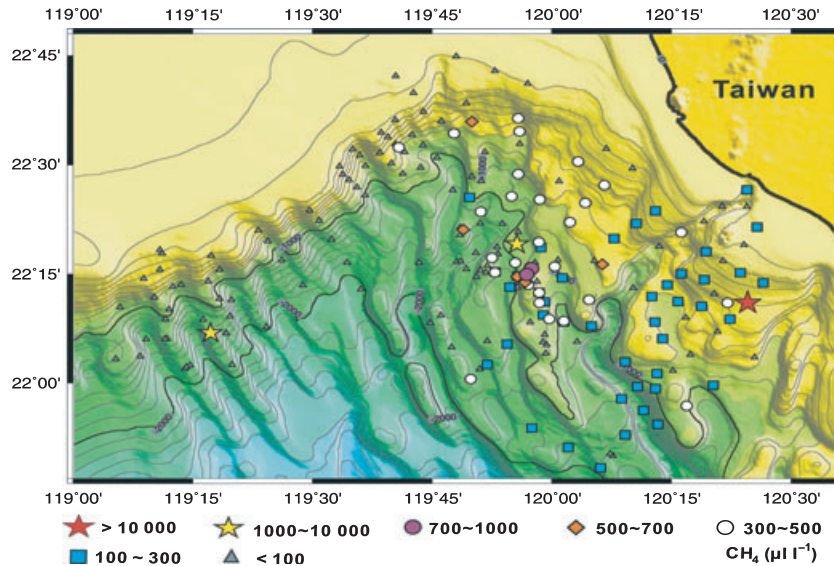


Fig. 4. The distributions of methane concentrations (in $\mu\text{l l}^{-1}$) of pore spaces of cored sediments (usually from depth of ca. 5–25 cm) in offshore southern Taiwan.

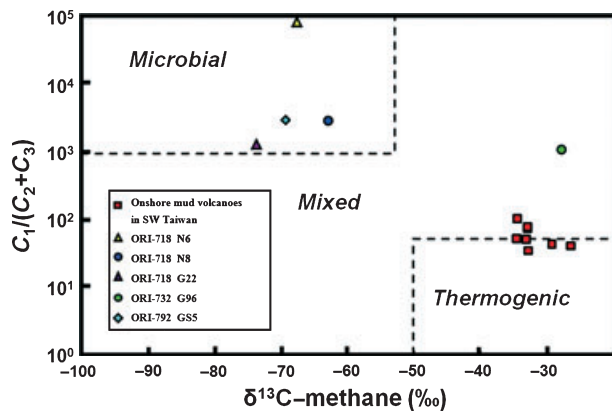


Fig. 5. Plot of the natural gas interpretative diagram combined the molecular and isotope compositional information (after Bernard *et al.* 1978). Gas compositions of onshore mud volcanoes from ChuKou Fault Zone are also plotted for comparison (data from Sun *et al.* 2010).

where the SMI depths are shallower (Fig. 3 and Table 5). Additionally, even though the SMI cannot be located at some sites (sites G3, G17, G19, N9, GH8, GH14, etc.), the sulfate flux can be used as a proxy methane flux. The proxy methane fluxes of sites G23 ($4.18 \times 10^{-2} \text{ mmol cm}^{-2} \text{ year}^{-1}$) of cruise ORI-697, N8 ($2.12 \times 10^{-2} \text{ mmol cm}^{-2} \text{ year}^{-1}$) of cruise ORI-718 and GH10 ($1.29 \times 10^{-2} \text{ mmol cm}^{-2} \text{ year}^{-1}$) of cruise ORI-758 revealed very high values compared to other gas hydrate and upwelling study areas (Borowski *et al.* 1996; Niewöhner *et al.* 1998; Dickens 2001). The high proxy methane fluxes indicate that there might be a methane-enriched source below the sea floor in this region. Based on other indicators, the methane-

Table 4 Carbon isotope data of methane and hydrocarbon compositions of selected samples.

Sample name	$\text{CH}_4 \delta^{13}\text{C}$, ‰ versus V-PDB	CH_4 ($\mu\text{l l}^{-1}$)	C_2H_6 ($\mu\text{l l}^{-1}$)	C_3H_8 ($\mu\text{l l}^{-1}$)	$\text{C}_1/(\text{C}_2 + \text{C}_3)$
ORI-718 N6	-67.8	64 263	0.75	b.d.l.	85 684
ORI-718 N8	-63.1	121 716	40.5	b.d.l.	3005
ORI-718 G22	-74.5	61 638	47.3	b.d.l.	1303
ORI-732 G96	-28.3	33 381	29.6	b.d.l.	1128
ORI-792 G55	-69.5	3882	1.30	b.d.l.	2986

b.d.l., below detection limit.

enriched source might be generated from the dissociation of gas hydrates (Lin *et al.* 2006; Liu *et al.* 2006).

As methane is not completely depleted above the SMI at sites N8, G96, H, G5A, and G55, methane emission into the water column might occur in the studied sediments (Table 3; Fig. 3). From Fig. 2 and Chuang *et al.* (2006), extremely high methane concentrations can also be observed in core top waters at these sites, so that methane discharge into the water column is highly probable as reported by Yang *et al.* (2006).

Parallel methane gradients found at the sites with different SMI depths

As mentioned in previous sessions, the calculated methane fluxes could be minimum values because of potential gas loss. An interesting phenomenon can be seen that methane profiles at sites GH6 and C reveal approximately parallel methane gradients below the SMI depth (Fig. 3). The parallel methane gradients result in similar calculated meth-

Cruise	Site	Ds of methane		Methane flux (mmol cm ⁻² year ⁻¹)	Ds of sulfate		Sulfate flux (proxy methane flux) (mmol cm ⁻² year ⁻¹)	
		(m ⁻² year ⁻¹)	φ		(m ⁻² year ⁻¹)	φ		
ORI-697	G1					8.14E-03	0.61	4.96E-04
	G3					7.74E-03	0.57	1.76E-03
	G5A	1.27E-02	0.61	2.36E-03		8.04E-03	0.60	3.85E-03
	G6					7.84E-03	0.58	3.24E-04
	G10					7.49E-03	0.55	8.27E-04
	G15					8.19E-03	0.61	1.99E-03
	G17					7.91E-03	0.59	7.48E-03
	G19					7.73E-03	0.57	6.15E-03
	G21					8.23E-03	0.62	6.14E-03
	G23	1.21E-02	0.58	1.16E-02		1.02E-02	0.76	4.18E-02
ORI-718	G22	1.28E-02	0.62	3.17E-03		8.36E-03	0.63	4.76E-03
	N8	1.26E-02	0.61	9.64E-03		8.12E-03	0.61	2.12E-02
	N6	1.32E-02	0.64	7.91E-04		8.37E-03	0.63	4.76E-03
	N4					7.64E-03	0.56	2.39E-03
	N9					7.46E-03	0.54	6.68E-04
ORI-758	GH3	1.36E-02	0.66	1.18E-03		8.74E-03	0.66	2.16E-02
	GH6	1.38E-02	0.67	1.78E-03		8.87E-03	0.67	4.44E-03
	GH7					8.37E-03	0.63	1.93E-03
	GH8					9.44E-03	0.71	1.12E-03
	GH10	1.47E-02	0.71	2.16E-03		9.44E-03	0.71	1.29E-02
	GH11					8.74E-03	0.66	1.79E-03
	GH13					9.60E-03	0.72	4.15E-03
	GH14					1.24E-02	0.86	9.17E-04
	GH15					1.04E-02	0.77	1.88E-03
	GH18					9.92E-03	0.74	2.31E-03
ORI-765	GH19					1.04E-02	0.77	3.12E-03
	GH20					8.03E-03	0.60	1.69E-03
	A	1.26E-02	0.61	1.52E-03		8.14E-03	0.61	1.53E-02
	C	1.21E-02	0.58	1.22E-03		7.81E-03	0.58	8.65E-03
	D	1.32E-02	0.64	2.66E-04		8.49E-03	0.64	6.08E-03

Table 5 Calculated diffusive flux of methane and sulfate.

Data of porosity ϕ is from Jiang *et al.* (2006) and Lin *et al.* (2006) and sulfate data from Lin *et al.* (2006).

ane fluxes (1.78 versus 1.22×10^{-3} mmol cm⁻² year⁻¹) (Table 5), although they exhibit different SMI depths (ca. 3.2 and 1.5 m, respectively). Furthermore, the calculated sulfate fluxes do not show big differences for these two sites (4.44 versus 8.65×10^{-3} mmol cm⁻² year⁻¹) (Table 5). In contrast, the SMI depths of sites GH3 and C are similar (ca. 1.5 m), but the calculated sulfate flux at site GH3 (2.16×10^{-2} mmol cm⁻² year⁻¹) is more than one order of magnitude higher than the value obtained at site C (8.65×10^{-3} mmol cm⁻² year⁻¹) (Table 5). The phenomenon is different from the conclusion of a previous study that the shallower depths of the SMI can be used to imply the higher methane fluxes under the sea floor (Borowski *et al.* 1996). It is likely that the SMI depths should not be used to infer the relative amount of the methane flux under the seafloor for some special cases. Hence, a model is proposed (Fig. 6) to explain this interesting observation.

Usually, the top of the gas hydrate stability zone is set at the seafloor. As methane concentration within the hydrate stability boundary in upper sediment is not sufficient to

form gas hydrate, the top of the actual gas hydrate occurrence zone usually does not coincide with the top of gas hydrate stability zone. Only if the mass fraction of methane dissolved in liquid is equal to methane solubility in seawater, can gas hydrate form in marine sediments (Xu & Ruppel 1999). Although it is not possible to quantify whether the amount of methane reaches methane solubility in deeper sediments because of the constraint of the sampling equipment, it is here proposed that the methane concentration in sulfate reduction zone is lower than methane solubility. Therefore, the top of hydrate occurrence zone, represented by a white line in Fig. 6, is greater than the depth of the SMI represented by a yellow line. If the chimneys and/or faults penetrate the sediments, gas hydrates will be dissociated and the top of hydrate occurrence zone will be elevated beside the chimneys and/or faults. Furthermore, it is proposed that the methane concentrations are saturated in the same layer of the top of hydrate occurrence zone because the methane concentrations had reached the methane solubility area in the hydrate occurrence zone. It is also possible to reasonably assume that

the sediment conditions are similar at nearby positions, thus methane can diffuse upward at the same rate. If methane can transfer to the sediment surface at the same rate, then the SMI depths, where methane is depleted, would be parallel to the upper boundaries of the hydrate occurrence zone. Consequently, it is possible to observe different depths of the SMI below seafloors and parallel methane gradients, i.e., similar methane flux, from the adjacent coring sites as shown in Fig. 6.

The distribution of methane fluxes and its tectonic implications

The distribution of methane concentrations in the pore spaces of cored sediments are shown in Fig. 4. In comparison with Fig. 2, both figures show that sites with higher methane concentrations are distributed in three main areas, following the tectonic description of Lin *et al.* (2008) in this region: one is in the upper slope (sites H and G96), another is in the lower slope (sites GH3, GH6, GH10, GH16, A, C, D, N6, N8, G23, G22, and G5A) and the other is in the South China Sea continental slope (site GS5) (Fig. 1). *In situ* organic matter might not be able to provide such high methane fluxes in this study area, because the TOC content in the area is <1%. It is important to find the origin of methane and if there are other methane sources under the sea floor. Lin *et al.* (2009) proposed that deeper-seated thermogenic gas may migrate

upwards, via deep cutting fault zones, to reach the shallow subsurface beneath the seafloor in the South China Sea continental slope. The existence of deeper thermogenic gas beneath the South China Sea continental margin is attested by the F gas field discovered in the shelf and near the shelf break (Lin *et al.* 2009). Biogenic gas is the main component for gas found at site GS5 as indicated by its isotopic value of $\delta^{13}\text{C}_{\text{CH}_4}$ to be around -69.5% (Table 4). This microbial signal may be the result of secondary migration as only a very shallow sediment sample was recovered beneath the seafloor (approximately 42 cm). Further work is warranted to determine the possible contribution of thermogenic gas to the gas hydrate stability zone beneath the South China Sea continental slope. Besides, proxy methane fluxes at sites GH3, GH10, A, G23, and N8 are one order of magnitude higher than sites GH6, C, D, G22, N6, and G5A. However, those sites are all distributed in the active margin and have shallow depths of the SMI and biogenic sources of methane (Figs 4 and 5). A dense grid of multichannel seismic profiles in the South China Sea continental slope and lower-slope domain of the accretionary wedge offshore SW Taiwan has been analyzed by Lin *et al.* (2008, 2009). The lower-slope domain can be further divided into a frontal segment and a rear segment. The frontal segment is characterized by anticlines and blind thrusts and the northern rear segment is characterized by a thrust penetrating through to the seafloor (Lin *et al.* 2008). The blind thrust in the frontal segment possibly forms a conduit for methane discharge and gas can accumulate in anticlines to form hydrates or gassy sediments. Nevertheless, gas cannot have time and space to accumulate in the northern rear segment, because methane discharges more easily through the thrust to the water column. Therefore, although it was possible to detect most sites with high methane concentrations in active margin, distinct tectonic settings result in varied proxy methane fluxes.

Liu *et al.* (2006) showed the distribution of BSRs in offshore SW Taiwan. BSRs can be recognized both in the active margin and in the passive margin, but the abovementioned sites with higher methane concentrations are mainly detected in the active margin and only site GS5 is found in the passive margin. These results suggest that tectonic setting has a strong effect on the stability of gas hydrates (Fig. 7). It is here proposed that gas hydrates are stable and the methane gas may have been mainly microbial in origin before Taiwan arc-continent collision occurred. Most sites with lower methane concentrations have been found in the South China Sea continental slope except site GS5. It might be because of the many fold-and-thrust structures developed in the lower slope that gas hydrates are not stable along those structures and so methane, from dissociated gas hydrates, can easily migrate to the surface area or water column

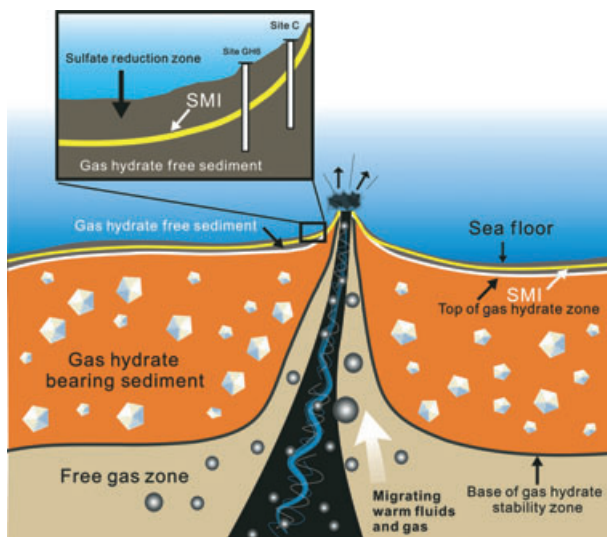


Fig. 6. Schematic diagram describes the observed geochemical profiles of Sites C and GH6, which show parallel methane gradients and different depths of the sulfate–methane interface represented by the yellow line. If chimneys and/or faults penetrate sediments, gas hydrates will be dissociated and then, the top of hydrate occurrence zone represented by the white line beside the chimneys and/or faults will be elevated. See Discussion in the text.

through the fractures or fluid conduits, e.g., sites GH3, GH6, GH10, GH16, A, C, D, N6, N8, G23, G22, and G5A. The analyzed $\delta^{13}\text{C}_{\text{CH}_4}$ values of cored sediments in the lower slope mainly fall into the area of microbial region (Fig. 5). In the upper slope, the shallow water depths cause pressure and temperature conditions beyond the hydrate stability boundary. Mud volcanoes and/or gassy sediments can still be detected in the upper slope (Chiu *et al.* 2006; Lin *et al.* 2008) (Fig. 7). Taking sites G96 and H, which are located at one of the mud volcano areas, exhibiting high methane concentration might result from destabilized gas hydrates. The $\delta^{13}\text{C}_{\text{CH}_4}$ value of site G96 lies in the mixing zone between biogenic and thermogenic sources (Fig. 5). Thermogenic gases might be introduced from deeper source through well-developed thrust faults in this region. After secondary migrations and mixing with shallow biogenic gases, the $\text{C}_1/(\text{C}_2 + \text{C}_3)$ ratios become enriched in C_1 at site G96 (Fig. 5). This supports the idea that the tectonic environments control the gas sources, the stabilities of gas hydrates in this region.

CONCLUSIONS

- (1) High methane concentrations in both bottom waters and cored sediments are predominantly distributed in active margins, offshore SW Taiwan. The only exception in a passive margin setting can be found at site GS5 of cruise ORI-792.
- (2) Different cruises have replicated sampling sites at different times indicating that methane venting areas of offshore SW Taiwan are widespread, and there is a sustained methane venting source underneath each site.
- (3) The anomalously high methane flux, which may be underestimated because of possible gas loss during/after sampling, and proxy methane flux have been found at sites G23 of cruise ORI-697, N8 of cruise ORI-718, GH3, GH10 of cruise ORI-758 and A of cruise ORI-765 in this study.
- (4) According to parallel methane gradients and different depths of the SMI at some duplicate sites, methane probably migrated to surface sediments from the same reservoir with the same diffusive rates.

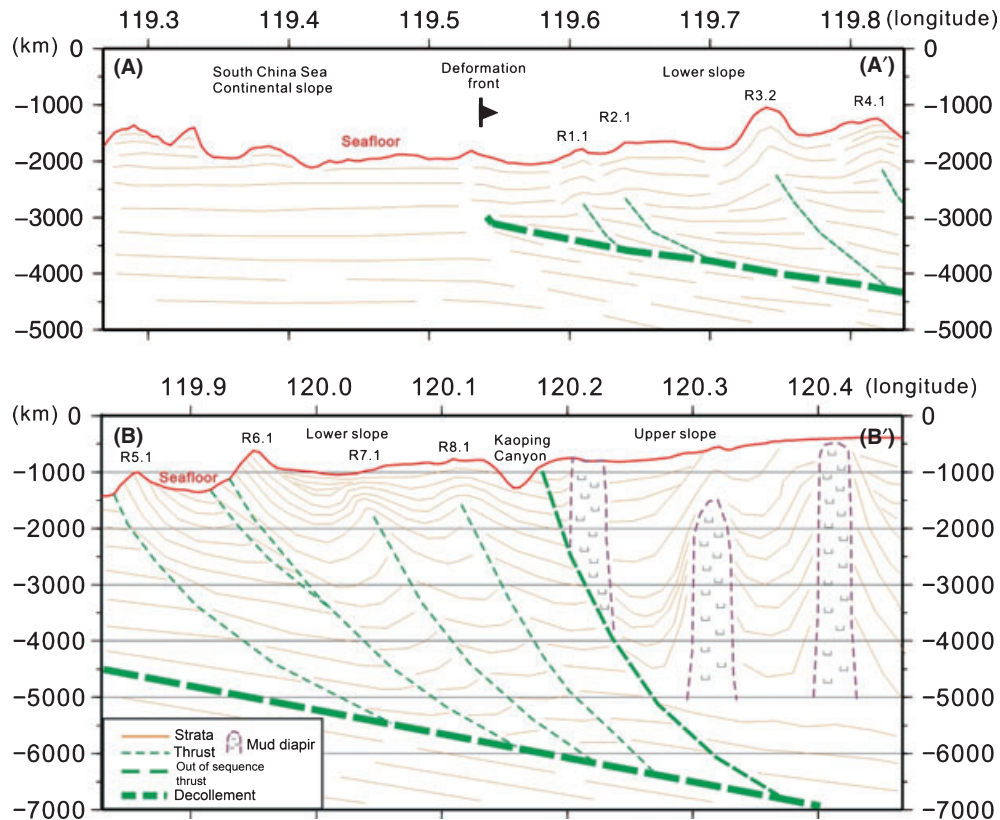


Fig. 7. Two schematic depth profiles along AA' and BB' transects shown in Fig. 1. The stratigraphic architecture and geological structures along the profiles are drawn from nearby seismic sections to demonstrate the major geological features along the two transects. In the accretionary wedge, eastward of the deformation front, folds-and-thrusts are predominant structures in the lower-slope domain whereas mud diapiric structures predominate in the upper-slope domain. The bathymetric ridges in the lower-slope domain correspond to underlying active folding and thrusting structures marked by a name for each structure (e.g., R7.1) as detailed in Lin *et al.* (2008). The bathymetric ridges westward of the deformation front and in the continental slope of the South China Sea are remnant ridges sided by erosional gullies.

- (5) The $\delta^{13}\text{C}$ values of CH_4 gases range from -28.3‰ to -74.5‰ . Except for the site G96, most carbon isotopic compositions of methane show that a biogenic gas source is dominant at shallower depth. However, site G96 close to onshore mud volcanoes exhibit much heavier carbon isotopic composition, indicating some thermogenic gases might be introduced from a deeper source through the fracture/fault zones in the tectonically active region of the studied area.
- (6) Based on these results and the distribution of BSRs, the methane concentrations and fluxes might be strongly controlled by the stability of hydrates under different tectonic settings, i.e., the lower slope, upper slope, and the South China Sea continental slope in offshore of SW Taiwan.

ACKNOWLEDGEMENTS

We thank the crew of the R/V Ocean Research Vessel I and all assistants and students on board for their help in sample collections and preparation. Dr C.-S. Liu provided seismic data and useful suggestions during different stages of this project. Dr Glen Snyder and one anonymous reviewer gave constructive comments. The editor, Prof. R. Worden, carefully edited and improved the manuscript. Central Geological Survey of Taiwan, R.O.C. provided financial supports for this study (5226902000-05-95-02; 5226902000-05-96-02).

REFERENCES

- Bernard BB, Brooks JM, Sackett WM (1978) Light hydrocarbons in recent Texas continental shelf and slope sediments. *Journal of Geophysical Research*, **83**, 4053–61.
- Berner RA (1980) *Early Diagenesis: A Theoretical Approach*. Princeton University Press, Princeton. pp. 241.
- Borowski WS, Paull CK, Ussler W (1996) Marine pore-water sulfate profiles indicate in situ methane flux from underlying gas hydrate. *Geology*, **24**, 655–8.
- Borowski WS, Paull CK, Ussler W (1999) Global and local variations of interstitial sulfate gradients in deep-water, continental margin sediments: sensitivity to underlying methane and gas hydrates. *Marine Geology*, **159**, 131–54.
- Chao H-C, You C-F, Sun C-H (2010) Gases in Taiwan mud volcanoes: chemical composition, methane carbon isotopes, and gas fluxes. *Applied Geochemistry*, **25**, 428–36.
- Chen N-C, Yang TF, Hong W-L, Chuang P-C, Chen H-C, Lin S, Matsumoto R, Hiruta A, Yang T, Jiang S-Y, Chung S-H, Wang Y (2008) The carbon isotopes of DIC and methane gas from gas hydrate potential area offshore SW Taiwan. *Eos Trans American Geophysical Union, Fall Meeting*. 89(53), Suppl. Abstract OS33A-1320.
- Chi W-C, Reed DL, Liu C-S, Lundberg N (1998) Distribution of the bottom simulating reflector in the offshore Taiwan collision zone. *Terrestrial, Atmospheric and Oceanic Sciences*, **9**, 779–93.
- Chiu J-K, Tseng W-H, Liu C-S (2006) Distribution of gassy sediments and mud volcanoes offshore southwestern Taiwan. *Terrestrial, Atmospheric and Oceanic Sciences*, **17**, 703–22.
- Chow J, Lee J-S, Sun R, Liu C-S, Lundberg N (2000) Characteristics of the bottom simulating reflectors near mud diapirs: offshore southwestern Taiwan. *Geo-Marine Letters*, **20**, 3–9.
- Chuang P-C, Yang TF, Lin S, Lee H-F, Lan T-F, Hong W-L, Liu C-S, Chen J-C, Wang Y (2006) Extremely high methane concentration in bottom water and cored sediments from offshore southwestern Taiwan. *Terrestrial, Atmospheric and Oceanic Sciences*, **17**, 903–20.
- Dickens GR (2001) Sulfate profiles and barium fronts in sediment on the Blake Ridge: present and past methane fluxes through a large gas hydrate reservoir. *Geochimica et Cosmochimica Acta*, **65**, 529–43.
- Hensen C, Zabel M, Pfeifer K, Schwenk T, Kasten K, Riedinger N, Schulz HD, Boetius A (2003) Control of sulfate pore-water profiles by sedimentary events and the significance of anaerobic oxidation of methane for the burial of sulfur in marine sediments. *Geochimica et Cosmochimica Acta*, **67**, 2631–47.
- Huang C-Y, Chien C-W, Zhao M, Li H-C, Iizuka Y (2006) Geological study of active cold seeps in the syn-collision accretionary prism Kaoping slope off SW Taiwan. *Terrestrial, Atmospheric and Oceanic Sciences*, **17**, 679–702.
- Iversen N, Jørgensen BB (1993) Diffusion coefficients of sulfate and methane in marine sediments: influence of porosity. *Geochimica et Cosmochimica Acta*, **57**, 571–8.
- Jiang W-T, Chen J-C, Huang B-J, Chen C-J, Lee Y-T, Huang P-R, Lung C-C, Huang S-W (2006) Mineralogy and physical properties of cored sediments from the gas hydrate potential area of offshore southwestern Taiwan. *Terrestrial, Atmospheric and Oceanic Sciences*, **17**, 981–1007.
- Kvenvolden KA (1998) A primer on the geological occurrence of gas hydrate. In: *Gas Hydrates: Relevance to World Margin Stability and Climate Change* (eds Henriot JP, Mienert J), **137**, 9–30. Geological Society of London Special Publication, London.
- Kvenvolden KA, Lorenson TD (2000) Methane and other hydrocarbon gases in sediment from the southeastern North American continental margin. In: *Proceedings of the Ocean Drilling Program, Scientific Results* (ed. Paull CK et al.), **164**, 29–36. College Station, Texas, Ocean Drilling Program.
- Lee H-F, Yang TF, Lan TF, Song S-R, Tsao S (2005) Fumarolic gas composition of the Tatun Volcano Group, northern Taiwan. *Terrestrial, Atmospheric and Oceanic Sciences*, **16**, 843–64.
- Lee H-F, Yang TF, Lan TF, Chen C-H, Song S-R, Tsao S (2008) Temporal variations of gas compositions of fumaroles in the Tatun Volcano Group, northern Taiwan. *Journal of Volcanology and Geothermal Research*, **178**, 624–35.
- Lin S, Hsieh W-C, Lim Y-C, Yang TF, Liu C-S, Wang Y (2006) Methane migration and its influence on sulfate reduction in the Good Weather Ridge region, South China Sea continental margin sediments. *Terrestrial, Atmospheric and Oceanic Sciences*, **17**, 883–902.
- Lin AT, Liu C-S, Lin C-C, Schnürle P, Chen G-Y, Liao W-Z, Teng LS, Chuang H-R, Wu M-S (2008) Tectonic features associated with the overriding of an accretionary wedge on top of a rifted continental margin: an example from Taiwan. *Marine Geology*, **255**, 186–203.
- Lin CC, Lin AT, Liu C-S, Chen G-Y, Liao W-Z, Schnürle P (2009) Geological controls on BSR occurrences in the incipient arc-continent collision zone off southwest Taiwan. *Marine and Petroleum Geology*, **26**, 1118–31.
- Liu C-S, Schnürle P, Wang Y, Chung S-H, Chen S-C, Hsuiuan T-H (2006) Distribution and characters of gas hydrate offshore of southwestern Taiwan. *Terrestrial, Atmospheric and Oceanic Sciences*, **17**, 615–44.

- Lorenson TD, Collett TS (2000) Gas content and composition of gas hydrate from sediments of the southeastern North American continental margin. In: *Proceedings of the Ocean Drilling Program, Scientific Results* (ed. Paull CK *et al.*), **164**, 37–46. College Station, Texas, Ocean Drilling Program.
- Milkov AV (2004) Global estimates of hydrate-bound gas in marine sediments: how much is really out there? *Earth Science Reviews*, **3–4**, 183–97.
- Milkov AV, Dickens GR, Claypool GE, Lee YJ, Borowski WS, Torres ME, Xu W, Tomaru H, Trehu AM, Schultheiss P (2004) Co-existence of gas hydrate, free gas, and brine within the regional gas hydrate stability zone at Hydrate Ridge (Oregon margin): evidence from prolonged degassing of a pressurized core. *Earth and Planetary Science Letters*, **222**, 829–43.
- Niewöhner C, Hensen C, Kasten S, Zabel M, Schulz HD (1998) Deep sulfate reduction completely mediated by anaerobic methane oxidation in sediments of the upwelling area off Namibia. *Geochimica et Cosmochimica Acta*, **62**, 455–64.
- Pecher IA (2002) Gas hydrates on the brink. *Nature*, **420**, 622–3.
- Schnürle P, Hsuan T-H, Liu C-S (1999) Constraints on free gas and gas hydrate bearing sediments from multi-channel seismic data, offshore southwestern Taiwan. *Petroleum Geology of Taiwan*, **33**, 21–42.
- Schnürle P, Hsuan T-H, Wang T-K, MacIntosh K, Liu C-S, Reed D, Nakamura Y (2002) Characteristics of gas hydrate and free gas offshore southwestern Taiwan: preliminary results from a combined seismic reflection/refraction analysis. *Petroleum Geology of Taiwan*, **35**, 1–34.
- Sivan O, Schrag DP, Murray RW (2007) Rates of methanogenesis and methanotrophy in deep-sea sediments. *Geobiology*, **5**, 141–51.
- Sloan ED Jr (1998) Physical/chemical properties of gas hydrates and application to world margin stability and climatic change. In: *Gas Hydrates: Relevance to World Margin Stability and Climate Change* (eds Henriot JP, Mienert J), **137**, 31–50. Geological Society of London Special Publication, London.
- Suess E, Torres ME, Bohrmann G, Collier RW, Greinert J, Linke P, Rehder G, Trehu A, Wallmann K, Winckler G, Zuleger E (1999) Gas hydrate destabilization: enhanced dewatering, benthic material turnover and large methane plumes at the Cascadia convergent margin. *Earth and Planetary Science Letters*, **170**, 1–15.
- Sun C-H, Chang S-C, Kuo C-L, Wu J-C, Shao P-H, Oung J-N (2010) Origins of Taiwan's mud volcanoes: evidence from geochemistry. *Journal of Asian Earth Sciences*, **37**, 105–16.
- Teng LS (1990) Geotectonic evolution of late Cenozoic arc-continent collision in Taiwan. *Tectonophysics*, **183**, 57–76.
- Xu W, Ruppel C (1999) Predicting the occurrence, distribution and evolution of methane gas hydrates in porous marine sediment. *Journal of Geophysical Research*, **104**, 5081–96.
- Yang TF (2008) Recent progress in the application of gas geochemistry: examples from Taiwan and the 9th International Gas Geochemistry Conference. *Geofluids*, **8**, 219–29.
- Yang TF, Chou C-Y, Chen C-H, Chyi LL, Jiang J-H (2003) Exhalation of radon and its carrier gases in SW Taiwan. *Radiation Measurements*, **36**, 425–9.
- Yang TF, Yeh G-H, Fu C-C, Wang C-C, Lan TF, Lee H-F, Chen C-H, Walia V, Sung Q-C (2004) Composition and exhalation flux of gases from mud volcanoes in Taiwan. *Environmental Geology*, **46**, 1003–11.
- Yang TF, Chuang P-C, Lin S, Chen J-C, Wang Y, Chung S-H (2006) Methane venting in gas hydrate potential area offshore of SW Taiwan: evidence of gas analysis of water column samples. *Terrestrial, Atmospheric and Oceanic Sciences*, **17**, 933–50.
- Yeh G-H, Yang TF, Chen J-C, Chen Y-G, Song S-R (2005) Fluid geochemistry of mud volcanoes in Taiwan. In: *Mud Volcanoes, Geodynamics and Seismicity* (Eds Martinelli G, Panahi B), pp. 227–37. Springer, Amsterdam.
- You C-F, Gieskes JM, Lee T, Yui T-F, Chen H-W (2004) Geochemistry of mud volcano fluids in the Taiwan accretionary prism. *Applied Geochemistry*, **19**, 695–707.